Deep Learning on a Novel Ising Model to Study Arctic Sea Ice Dynamics

Ellen Wang[1*]

[1] Horace Mann School, Bronx, NY, USA

***** Ellen_Wang@horacemann.org

Summary:

This research aims to model Arctic Sea Ice dynamics and contribute to climate change studies by combining the 100-year-old Ising model in statistical physics with modern deep learning methods. Upon a classical two-dimensional binary-spin Ising model, we introduce continuous spin values that capture the real-world ice-water phase transition, and a novel inertia factor that represents the natural resistance to any state change. We utilize this generalized model to simulate the sea ice evolution in a focus area in the Arctic region, by engaging the Metropolis-Hastings algorithm for Monte Carlo simulation and training a convolutional neural network to learn the Ising interaction parameters. Using the sea ice concentration data collected by the National Snow and Ice Data Center, our model proves to have strong explanatory power of capturing the sea ice transition patterns. The simulated images show striking similarity with the actual ice/water configurations, and two numerical measures calculated from the simulation results, the average ice coverage and the ice extent, match closely with the data statistics. Moreover, the Ising parameters predicted by the convolutional neural network demonstrate the substantial impact of the external forces, which can be further enriched and linked to the environmental factors in other global warming studies. Our findings validate the vast potential of the classical Ising model and the modern deep machine learning algorithms in climate change research. Our study also reveals the possibilities for future research efforts to further enhance the modeling of sea ice dynamics, a crucial indicator of global warming.

Keywords: *Ising model, continuous spin, Metropolis-Hastings algorithm, phase transition, deep learning, convolutional neural networks, Arctic sea ice, climate change*

Table of Contents

List of Figures

List of Tables

1 Introduction

The rapid loss of the Arctic sea ice over the past four decades has been an alarming phenomenon that points to drastic global warming, a serious challenge that calls for collective actions by the entire humankind. To accurately predict the Arctic sea ice evolution, which helps prepare for the subsequent environmental and economic impact, therefore has become an urgent task for researchers across many disciplines. The fact that the year 2023 has witnessed the most sizzling summer on record and has proved to be the hottest year in history adds even greater severity to such urgency. As an endeavor to fulfill this task, we innovate upon the classical Ising Model in statistical physics and train the Convolutional Neural Networks in Deep Learning to solve for Ising interaction parameters. Our study, which delivers excellent match between model simulations and actual observations, unleashes the power of classical physics models and deep learning methods in climate change research and presents ample possibilities to further enhance the modeling of the Arctic sea ice dynamics.

1.1 Ising model

The classical Ising Model (IM) is the backbone of this study. It was first formalized by physicists Ernst Ising and Wilhelm Lenz to explain the equilibrium and phase transition in magnetic systems. The one-dimensional (1-D) IM was solved by Ising in his 1924 thesis [1], which proves the non-existence of phase transition in the 1-D IM. In 1944, Lars Onsager [2] was able to solve the two-dimensional (2-D) square-lattice IM analytically. Contradictory to the 1-D case, Onsager identified that there exists a critical temperature $T_c = 2.27\ J/k_B$ when the phase transition happens in a 2-D IM. Later studies of IM in higher dimensions have been closely associated with various developments in advanced 20^{th}-century physics and mathematical theories, including the transfer-matrix method, quantum field theory, mean-field theory, etc.

Over the years, the IM has found wide success beyond physics. Specifically, the Kinetic IM [3], built upon the equilibrium version, has been proposed to analyze biology, environmental science, machine learning [4], social science, and economic and financial systems. These applications are usually implemented as a discrete time Markov chain of the spin lattice, with spin interactions bounded to finite distance. In biology and neuroscience, IM applications include but are not limited to the condensation of DNA, genetics [5], neuron spike [6], neuron activity in cell assemblies [7], and ligands to receptors binding in cells [8]. In environmental science, it has been employed to investigate land pattern dynamics [9] and the equilibrium configuration of ice melt ponds [10]. In social science, economics, and finance, the IM has been applied to research in urban segregation, crisis study [11], stability of money [12], etc.

1.2 Convolutional Neural Networks

Our study falls into a broad body of literature that employs Artificial Neural Networks (ANNs), or neural networks (NNs), a branch of artificial intelligence and machine learning inspired by the structure and functioning of the human brain. Most modern deep learning models are based on multi-layered ANNs. Interestingly, Ising model has been considered as the first non-learning recurrent neural network (RNN) architecture [13].

The Convolutional Neural Networks (CNNs) [14] deployed in this study are a specialized type of NNs used to analyze data with grid-like topology, which revolutionized computer vision in the 2010s [13] [14]. CNNs have gained much success in image and video recognition; they have also been widely applied to time series analysis, recommender systems, natural language processing, etc. The images of 2-D IM lattices are well-qualified candidates for CNN training, which are explored in this study. The theory and the specifics of the IM and the architecture of CNNs will be described in detail in Section 2 and 4.

1.3 Arctic sea ice

The reversible phase transition between water and ice makes the IM a great tool to study the dynamics of a surface region with the co-existence of both states. In this paper, we apply a 2-D IM lattice to study the dynamics of Arctic sea ice melting and freezing cycles, a major climate change indicator that is of significant environmental, economic and social significance.

Sea ice is undoubtedly an integral part of the Arctic Ocean and the earth. In the dark winter months, ice covers almost the entirety of the Arctic Ocean, and the ice extent—defined as the percentage of the areas that are covered by at least 15% ice—and the ice thickness typically reaches its peak around March. Starting in late spring, ice melting gradually exceeds water freezing due to higher temperatures and longer hours of sunlight exposure. Sea ice typically reaches the minimum extent and thickness in mid-September, when ice coverage can drop to under half of the winter maximum. After mid-September, sea water freezing starts to exceed ice melting, so ice coverage expands. This cycle repeats annually.

Ice coverage is widely acknowledged as a crucial indicator of global climate change. Albedo, the percentage of incident light reflected from the surface of the earth, is highly dependent on the ice extent. Light-colored ice or snow reflects more light than blue-colored liquid water; therefore, ice is essential to keeping the Arctic at a cooler temperature and subsequently maintaining the energy balance around the globe. If the energy balance is broken, as ice decline has been detected in recent years, the feedback loop effect may occur, i.e., less reflection and more absorption of solar energy, leading to even more ice loss and further global warming. Moreover, the Arctic ecosystem is directly impacted by the change in sea ice coverage, which, for instance, threatens the lives of polar bears and walruses who rely on sea ice for hunting and breeding.

Data recorded by the National Aeronautics and Space Administration (NASA) and the National Snow and Ice Data Center (NSIDC) since 1979 has shown substantial declines in both ice extent and thickness in the Arctic, despite the year-over-year fluctuations in either direction. The lowest Arctic sea ice extent was observed in September of 2012; between

2013 and 2022, the ice extent has been higher than the 2012 minimum, but still much lower than the average of the past four decades. 2023 has recorded the hottest year by a significant margin, with July 2023 reported as the hottest month on the earth. Some questions then come to us naturally: how does the Artic sea ice extent in 2023 compare to the 2012 level? And can our model simulations closely match the comparison observed in the real data? These questions will be addressed in Section 5.4.

2 Theoretical framework

2.1 Classical Ising model

The system described by an IM is a set of lattice sites, each having a spin that interacts with its neighbors. The Hamiltonian function [1] for the lattice σ in a standard IM is given as

$$H(\sigma) = -\sum_{<i,j>} J_{ij}\sigma_i\sigma_j - \sum_i B_i\sigma_i, \quad (1)$$

where σ_i represents the spin variables at site i, taking the values of +1 or -1, J_{ij} represents the interaction between sites, and B_i represents the interaction of the external field with the spin at site i. i and j range across the full lattice, which can be one, two or higher dimensions, and $<i, j>$ represents pairs of spins that interact with each other. In the usual scenario, each spin only interacts with its nearest neighbors, so $<i, j>$ sums over all adjacent sites. For example, in a simple 2-D IM, each spin interacts only with four sites that are directly left, right, above and below. J_{ij} is usually positive, meaning that adjacent spins are inclined to maintain the same value to achieve low energy.

In statistical physics, the configuration probability follows the Boltzmann distribution

$$P_\beta(\sigma) = \frac{e^{-\beta H(\sigma)}}{Z_\beta}, \quad (2)$$

where Z_β is the partition function:

$$Z_\beta = \sum_\sigma e^{-\beta H(\sigma)}, \quad (3)$$

and

$$\beta = (k_B T)^{-1}. \quad (4)$$

β is the inverse temperature; k_B is the Boltzmann constant; T is the IM temperature (it is called IM temperature in this paper to differentiate from the ambient temperature that will also be discussed for our sea ice freezing and melting studies).

The evolution of the kinetic IM runs through a series of spin flips over the lattice. The probability of each spin flip depends on whether such a flip increases or reduces energy. Mathematically the probability is determined by $e^{-\beta(H_\nu - H_\mu)}$, where H_ν and H_μ represent the Hamiltonian of the system before and after the flip. It can be easily seen that a higher IM temperature leads to more thermal fluctuations and greater randomness in the spin value distribution, while a lower IM temperature shows less fluctuations.

2.2 Continuous Spin Ising model

Most studies of the IM focus on binary values of the spins, i.e., σ_i takes values of +1 or -1 only. However, the sea ice data for each lattice location takes varying values between 0 and 1 that represent the percentage of ice coverage. Therefore, we generalize the IM to allow for continuous spin values that can take any real number between -1 and +1. This generalization enables the IM to examine more realistic systems, but also adds a high degree of complexity to the mathematical solutions. Past research has studied phase transitions and critical behaviors of the continuous IM [15], and recently, an IM with variable power-law spin strengths was studied with its rich phase diagram [16].

The Hamiltonian function of the continuous spin IM is represented by the same Equation (1). However, σ_i now takes continuous values between $+1$ and -1; $-J_{ij}\sigma_i\sigma_j$ reaches the minimum energy state if $\sigma_i = \sigma_j = +1$, or $\sigma_i = \sigma_j = -1$, as the energy of any other values of the pairs will be higher. The highest energy is observed when $\sigma_i = +1$, $\sigma_j = -1$, or vice versa. This numeric feature works ideally for an ice/water lattice: the most stable low energy state is either 100% water or ice, whereas ice next to water is the most unstable high energy state.

2.3 Monte Carlo simulation and inertia factor

The incorporation of the continuous spins also adds to the complexity of the Monte Carlo (MC) simulation of the IM lattice. In the classical binary spin IM, σ_i can only flip to $-\sigma_i$ in each simulation step, and therefore the absolute value of the change is always 2 no matter if the flip goes from -1 to +1 or from +1 to -1. In a continuous IM, the challenge of determining the post-flip numeric value of the new spin arises. In our approach, this new spin is implemented through a random number. However, what is the random distribution that the new spin value should follow? How does the spin value change, i.e. $\Delta\sigma_i$, affect the dynamics of the IM? To address these questions, we introduce an innovative inertia factor *I*, and the probability of each flip will be determined by

$$P_{flip} = e^{-\beta(H_\nu - H_\mu + I|\sigma'_i - \sigma_i|)}, \tag{5}$$

where H_ν and H_μ still represent the system Hamiltonian before and after the flip. The newly added $-I|\sigma'_i - \sigma_i|$ accounts for the energy needed to overcome the inertia of the spin change, and *I* is an IM parameter to be fitted. Intuitively speaking, this term represents the

natural resistance to state change, or can be thought of as the latent heat needed for the water/ice phase transition in classical thermodynamics.

Here is an example to illustrate the inertia effect. Starting with an initial spin value of 0.8, a flip to either 0.7 or 0.6 may result in the same system Hamiltonian value for the new lattice. However, we differentiate these two new states by assigning higher probability for the flip to 0.7 because the spin change is smaller. In Equation (5), $-I|\sigma'_i - \sigma_i|$ determines the distribution of new spin values, and in practice, it significantly improves the simulation results to match the observations.

In summary, the novelty of our IM is twofold: we introduce to the classical IM the continuous spin values and an inertia factor. These mathematical additions prepare us to study real-world Arctic sea ice dynamics while keeping the computational complexity tractable.

2.4 The inverse Ising problem: solved with convolutional neural networks

The key of CNNs are convolutional layers, which employ a mathematical operation called convolution. A convolutional layer consists of kernels, or filters. The kernels slide along the input grid and compute the weighted sums; a certain activation function is applied on these sums to produce outputs. In most CNNs, the convolutional layers are followed by pooling layers, which reduce the network size and generate a summary statistic from the outputs of the convolutional layers. For instance, max pooling is one of the most popularly used techniques, which calculates the maximum value within a neighboring rectangular area.

Various machine learning studies of the IM have been conducted based on CNNs [17], due to the tremendous power of CNNs on image recognition. Most of these studies focus on exploring the phase transitions near a critical temperature, while some of them involve generative neural networks such as variational autoencoders [18] or normalizing flows [19]. Our task in this study is slightly different, which is to solve the so-called inverse Ising problem [20]: given the start and end state images of the Ising lattices, how do we determine the IM interaction parameters (*J, B, I*)? In this paper, we will train a CNN deep learning model for this task, with detailed steps to be explained in Section 4.5.

3 Data description

Our study uses data from the "Near-Real-Time DMSP SSMIS Daily Polar Gridded Sea Ice Concentrations" (NRTSI) dataset [21] collected by the National Snow and Ice Data Center (NSIDC). It captures daily sea ice concentrations for both the Northen and Southern Hemispheres. The Special Sensor Microwave Imager/Sounder (SSMIS) on the NANA Defense Meteorological Satellite Program (DMSP) satellites acquires the near-real-time passive microwave brightness temperatures, which serve as inputs to the NRTSI dataset using the NASA Team algorithm to generate the sea ice concentrations.

The NRTSI files are in netCDF format. Each file of the Arctic region contains a lattice of 448 rows by 304 columns, covering a large earth surface area with the north pole at the center. Each grid cell represents an area of approximately 25 kilometers by 25 kilometers. The value for each grid cell is an integer from 0 to 250 that indicates the fractional ice coverage scaled by 250. 0 indicates 0% ice concentration; 250 indicates 100% ice concentration. The image of part of the NRTSI file on Sept 16th, 2022 is illustrated in Figure 1(a). In the map, white represents ice, blue represents water, and gray represents land. The exact north pole location is covered by a gray circular mask because of the limitation of the satellite sensor measurement caused by the orbit inclination and instrument swath.

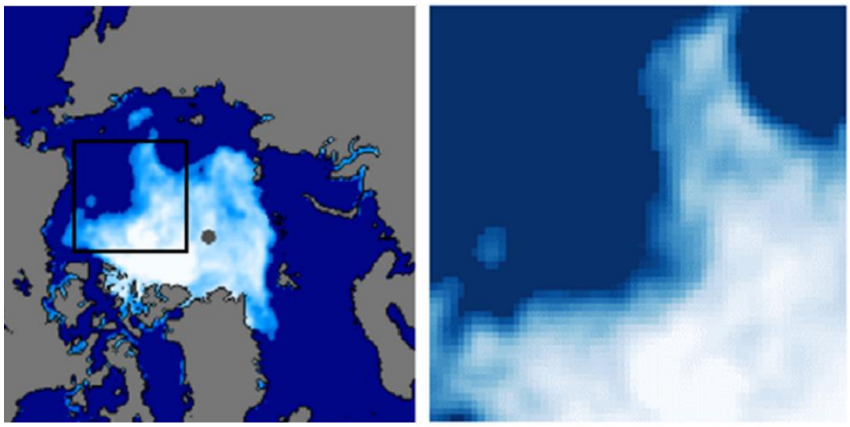

(a) (b)

Figure 1: (a) Part of the NRTSI data on Sept 16th, 2022; (b) The focus area for our research, a 60x60 square lattice covering approximately 2.25 million square kilometers.

For this research paper, we focus on studying a specific geographic region bounded by the black square in Figure 1(a), ranging from the East Siberian Sea (to the top of the box) and the Beaufort Sea (to the left of the box) to near the polar point; a zoom-in image of this focus area is shown in Figure 1(b) . This large square area is unobstructed by land or the north pole mask, making it an ideal field for the IM lattice setup. The area contains 60 rows and 60 columns in the data file, covering approximately 1500km x 1500km, or about 2.25 million square kilometers.

4 Ising model and convolutional neural networks setup

4.1 Ising model lattice

We first transform the NRTSI data of the focus region as shown in Figure 1 (b) to Ising-style data. A simple linear mapping is applied to convert integers from 0 to 250 to real numbers from -1 to +1. -1 indicates the cell is 100% ice; +1 indicates 100% water; 0 indicates 50%/50% coverage of water/ice. Each cell covers 25km x 25km of the total

1500km x 1500km focus region, and therefore a 60x60 matrix is initialized as the 2-D IM lattice for our study.

4.2 Simulation periods

Figure 2 (a) and (b) display an example of the initial and the final target states of an IM lattice simulation run. The simulation periods are chosen to be consistently half a month apart, for example, Sept 16th, 2022 in Figure 2 (a) and Oct 1st, 2022 in Figure 2 (b). This semi-monthly frequency is chosen to balance two considerations. First, the period is sufficiently long to allow for meaningful differentiation of the ice/water configuration between the start and the end dates; second, the period is not excessively too long and allows the IM simulation to mimic the daily water/ice configuration evolution on the interim dates between the start and the end, which is to be illustrated in Section 5.2.

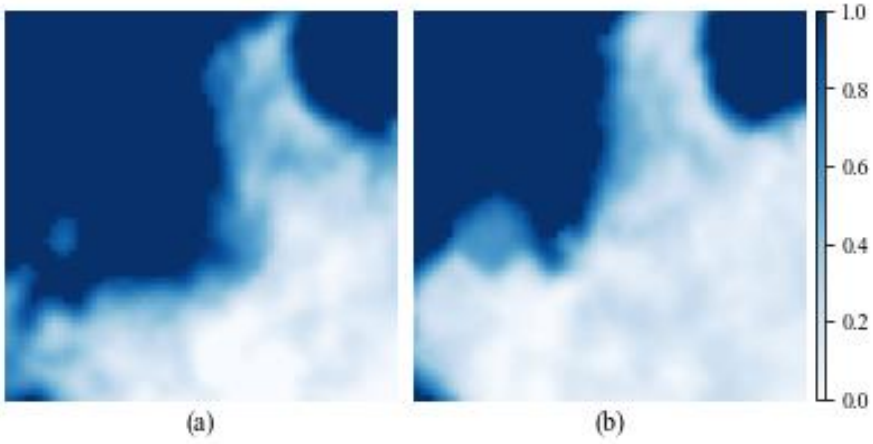

Figure 2: The initial and the final target states of an IM lattice simulation run. (a) shows the actual configuration observed in our focus area on Sept 16th, 2022 and (b) on Oct 1st, 2022. Each full simulation period is half a month. Blue color indicates water; white indicates ice. The darker the color on each cell, the higher the water concentration, as shown by the scale on the right.

4.3 Ising model parameters

In the IM Hamiltonian function, i.e., Equation (1), we set the following:

- σ_i is a real number between -1 and +1 for any cell *i* in our focus area.
- $<i, j>$ sums over all adjacent cells, so each spin interacts only with four sites that are directly left, right, above and below.
- J_{ij} is set to be constant within each simulation period across all cells.
- B_i is set to be time-invariant within each simulation period. However, in order to capture the real-world external force variation across locations, especially the environmental differences from the coast area to the north pole, B_i is set to be a linear function of x_i and y_i coordinates of cell *i*, i.e. $B_i = B_0 + B_x(x_i - x_0) +$

$B_y(y_i - y_0)$, where B_0 is the average B over the lattice, and x_0 and y_0 are the coordinates of the lattice center.

- I, the inertia factor, is set to be constant within each simulation period.
- β, the inverse Boltzmann temperature, is set to 1 without loss of generality.

4.4 Metropolis simulation steps

Various Monte Carlo (MC) methods have been developed for the IM simulation. Among them the most widely used are the Glauber dynamics and the Metropolis-Hasting algorithm. In our study, we follow the latter for the MC simulation of the IM lattice evolution. As described in Section 2.3, an inertia factor is introduced into our model and the generalized Metropolis-Hastings MC steps are below:

1. Select cell i at random from the 2-D lattice of the focus area. Let the spin value of this cell be σ_i.
2. Generate another random variable σ'_i between -1 and +1.
3. Compute the energy change ΔH_i from σ_i to σ'_i.
4. Compute the energy $I|\sigma'_i - \sigma_i|$ to overcome the inertia of changing the spin value at i.
5. Compute the total energy change $\Delta E = \Delta H_i + I|\sigma'_i - \sigma_i|$.
6. (a) If ΔE is negative, the energy change is favorable since the energy is reduced. The spin value change is therefore accepted to σ'_i.
   (b) If ΔE is positive, the probability of the spin flip is determined by the Boltzmann distribution. In this case, another random variable r between 0 and 1 is generated. If r is less than $P = e^{-\beta \Delta E}$, the spin value change is accepted; otherwise, the change is rejected and the spin value at i stays at σ_i.

For each semi-monthly simulation period, we repeat the above MC steps 50,000 times. As the lattice of our focus area has 3,600 cells, this repetition allows approximately 14 flip tries for each cell, or roughly once per day. This specific repetition number is an intuitive pick, which takes into account the computational complexity of the algorithm. Obviously, other choices of the repetition number can be considered as well. The fitted parameter values (J, B_0, B_x, B_y, I) might vary with different repetition numbers.

4.5 Architecture of the convolutional neural networks

In this research, we employ a CNN model to solve the inverse Ising problem; that is, to find the best-fit Ising parameters (J, B_0, B_x, B_y, I) based on the initial and final states of each simulation period. This CNN model is implemented with the Tensorflow/Keras package in Python.

The architecture of our CNN is drawn in Figure 3. It starts with the input layer, which consists of two images of shape (60, 60, 2), representing the start and end state images

respectively. It is followed by four convolutional layers with a kernel shape (3, 3). The filter counts from 16 in the first convolutional layer to 32, 64, and 128 in the last convolutional layer. Zero padding and strides (1, 1) are used to ensure coverage of the entire input grid. Each of the convolutional layers applies a Leaky Rectified Linear Unit (LeakyReLU) activation function. Every convolutional layer is followed by a max pooling layer of pool size (2, 2) that summarizes the crucial features and reduces the layer size. The outputs of the last max pooling layer are flattened and followed by a fully connected dense layer with LeakyReLU activation. Then, a dropout layer with dropout ratio 20% is applied to avoid overfitting. The outputs are fed to the final dense layer with linear activation. The number of neurons of the final dense layer is set to be 5, the same as the number of IM parameters to be solved. It is worth noting that our CNN model differs from most of the CNNs used for classification tasks, as our targets are the continuous Ising parameters instead of discrete categorical labels. This is the reason why we choose the activation function of the final layer as linear, rather than the more popular choices such as Sigmoid in classification tasks. The total number of trainable parameters stays at 213,101, making this a relatively small deep learning algorithm that can be trained on the CPU of a personal computer.

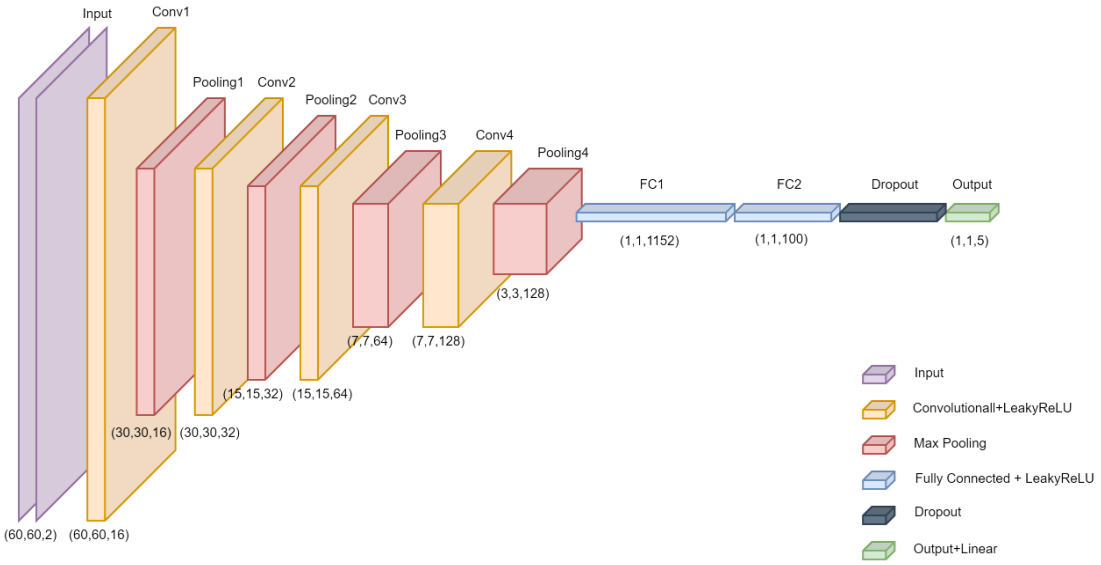

Figure 3: Architecture diagram of the CNN model to solve the inverse Ising problem. The function of each layer is labeled on the top; the shape of neurons at the bottom.

Training neural networks requires a substantial amount of data. In our study, these data are generated following the simulation steps described in previous subsections. To be specific, we start with the Ising lattice at the initial state of a simulation period and randomly select 10,000 set of parameters (J, B_0, B_x, B_y, I); for each set of parameters, we run the Metropolis simulation steps as described in section 4.4. As a result, we generate 10,000 sets of training samples corresponding to each of the initial states. An example of the training sample

corresponding to the initial state of the focus area on Sept 16th, 2022 and Ising parameters ($J = 2.31,\ B_0 = -14.5, B_x = -6.15, B_y = 0.07, I = 9.93$) is illustrated in Figure 4. Compared with Figure 2, this training sample apparently happens to correspond to a much faster freezing cycle than the actual observation.

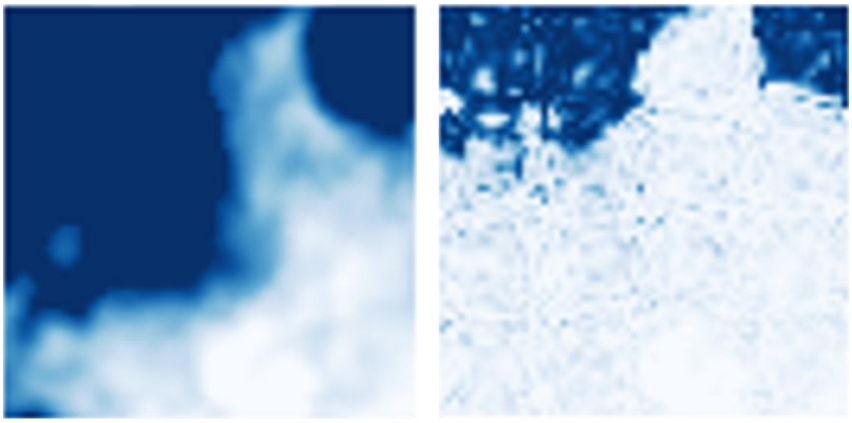

Figure 4: A CNN training sample pair. (a) is the initial state on Sept 16th, 2022 and (b) the final state on Oct 1st, 2022; the simulation is based on IM parameters ($J=2.31, B_0=-14.5, B_x=-6.15, B_y=0.07, I=9.93$).

These generated Ising configuration pairs for simulation periods from Jun 16th of each year to Jan 1st of the next year are passed as the inputs to our CNN model. As a supervised learning process, the target of our CNN model is set to be the corresponding Ising parameters (J, B_0, B_x, B_y, I). The model is trained with the *Adaptive Moment Estimation (ADAM)* optimizer and the loss function is set to be the *Mean Square Error*, a typical choice for regression models. After the model is completely trained, estimating the best-fit Ising parameters for each of our study periods is straightforward: we simply pass the observed initial and end state sea ice configuration images as inputs to the CNN model, which predicts and returns the respective Ising parameters (J, B_0, B_x, B_y, I) as outputs.

5 Results

Combining the CNN deep learning method with the continuous spin IM that incorporates a novel inertia factor, we are able to simulate the dynamics of the sea ice/water transition for the focus Arctic Sea area. Thanks to the publicly accessible NRTSI data, we can conduct the simulation and training for every year in the past four decades.

5.1 Simulation results for 2022

Naturally, our experiment starts with the year 2022, for which the most recent full year data are available.

Figure 5 shows the semi-monthly NSIDC sea ice images of our focus area from June 16th, 2022 to Jan 1st, 2023. As can be seen, the melting cycle starts from June 16th and goes until Sept 16th, and the freezing cycle from Sept 16th to year end. Prior to June 16th, the region is almost fully covered by ice, so the IM simulation will be trivial. This is why we set the simulation start date on June 16th of each year. During the period of June 16th to Dec 16th, every succeeding image shows considerable ice coverage difference from the previous date while retaining certain core features. This semi-monthly frequency choice allows our IM simulation to capture the essence of the evolution dynamics without overfitting the model.

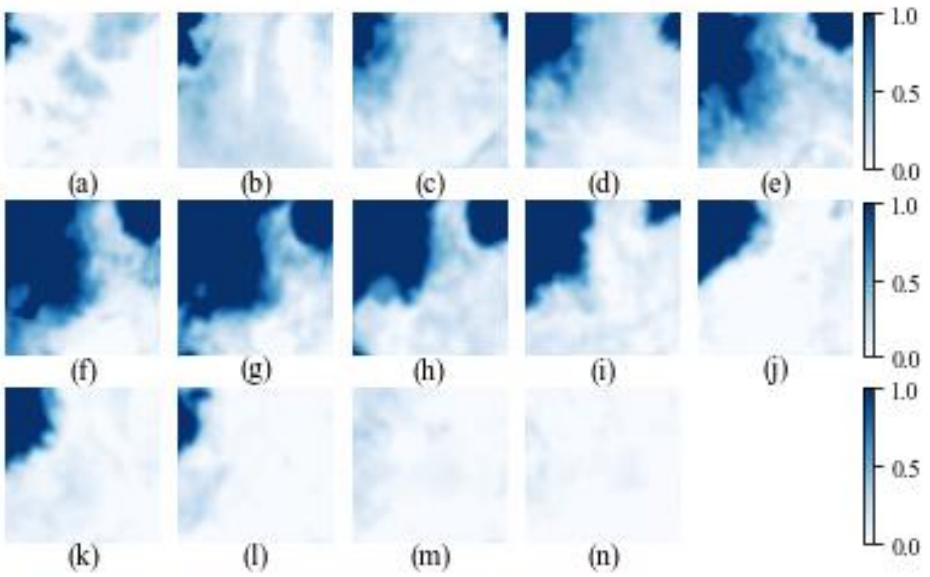

Figure 5: The actual semi-monthly evolution of sea ice in our focus area in 2022: (a) June 16th, (b) July 1st, (c) July 16th, (d) Aug 1st, (e) Aug 16th, (f) Sept 1st, (g) Sept 16th, (h) Oct 1st, (i) Oct 16th, (j) Nov 1st, (k) Nov 16th, (l) Dec 1st, (m) Dec 16th, 2022, and (n) Jan 1st, 2023.

The Ising parameters ($J,\ B_0, B_x, B_y, I$) predicted by the CNN model for each simulation period in 2022 are shown in Table 1. The spin interaction coefficient J and the inertia factor I are relatively stable across periods. On the other hand, the external force parameters $B_0, B_x,$ and B_y display large variations across different time periods. In particular, the average force B_0 is positive from June 1st to Sept 16th but turns negative afterwards, which can be explained intuitively by the seasonal ambient temperature as the dominant external factor for ice/water dynamics. Ambient temperature is not the only factor, though. Arctic temperature usually peaks in July/August while B_0 remains positive and ice melting continues through mid-September. This lagging effect could be explained by other environmental effects such as albedo or jet streams but is beyond the scope of this study.

	6/16 to 7/1	7/1 to 7/16	7/16 to 8/1	8/1 to 8/16	8/16 to 9/1	9/1 to 9/16	9/16 to 10/1	10/1 to 10/16	10/16 to 11/1	11/1 to 11/16	11/16 to 12/1	12/1 to 12/16	12/16 to 1/1/2023
J	2.1	2.6	2.9	2.6	2.5	2.5	2.3	2.4	3.5	2.1	2.6	2.3	2.8
B0	2.9	0.5	5.1	7.7	2.8	4.0	-7.1	-12.1	-30.0	-9.4	-18.6	-11.5	-28.0
Bx	3.5	-16.9	-14.9	2.7	-10.6	-7.6	-0.7	-4.1	-28.7	6.8	-1.9	-4.9	-4.3
By	-9.0	6.5	-4.7	3.4	-3.9	1.7	4.7	-6.2	-12.8	-34.5	-12.0	4.3	11.6
I	7.6	10.4	12.1	10.6	9.8	10.2	9.2	9.7	15.4	8.5	11.2	9.3	11.9

Table 1: CNN predicted Ising parameters for the 2022 sea ice evolution.

The simulated sea ice images for each 2022 period are shown in Figure 6 utilizing the CNN predicted Ising parameters in Table 1. These images exhibit excellent similarity to Figure 5, demonstrating the strong explanatory power of our Ising model. Nevertheless, our model is far from being perfect. Upon close inspection, The images in Figure 5 and Figure 6 do reveal discrepancies, especially as shown in image (d) and (e) for Aug 1st and 16th, 2022 respectively, where the actual ice configurations display significant irregularity compared to the prior period. While an IM with simple parameterization encounters difficulties in describing these local irregularities, it is feasible to include a richer set of parameters or to employ more complicated parametric functional forms at the potential cost of overfitting. In this paper, we keep our Ising model tractable and accept these local discrepancies.

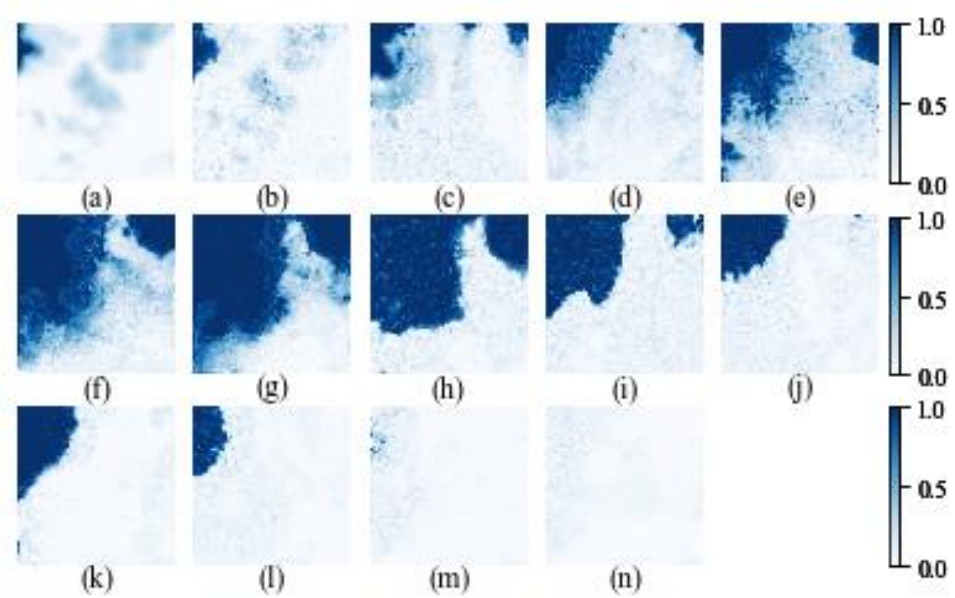

Figure 6: The simulated semi-monthly evolution of sea ice for our focus area in 2022. (a) is the actual image on June 16th, 2022; (b) - (n) are simulated images on (b) July 1st, (c) July 16th, (d) Aug 1st, (e) Aug 16th, (f) Sept 1st, (g) Sept 16th, (h) Oct 1st, (i) Oct 16th, (j) Nov 1st, (k) Nov 16th, (l) Dec 1st, (m) Dec 16th, 2022, and (n) Jan 1st, 2023.

To quantify the similarity between the IM simulations and the observations, we compute two key numerical measures for our focus area: the average ice coverage percentage, i.e., the mean of the ice coverage percentage over the lattice, and the ice extent, i.e., the percentage of areas that are covered by at least 15% ice. The comparison results are shown

in Figure 7. As anticipated, we see an excellent match in both figures as a result of the superior explanatory power of our IM, although the results do show marginal but non-trivial discrepancy. It is interesting to note that the simulated average ice coverage is usually slightly higher than the actual measures, but the simulated ice extent is slightly lower than the actual, a pattern that can be further investigated in future research.

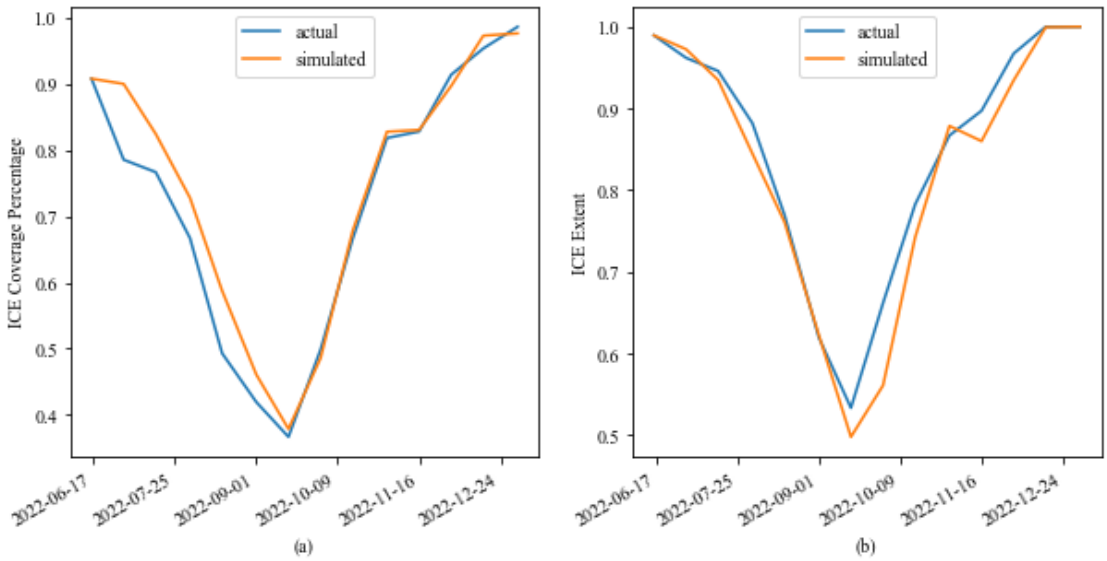

Figure 7: (a) The average ice coverage percentage in our focus area from June 16th, 2022 to Jan 1st, 2023; (b) The sea ice extent (the percentage of areas with at least 15% ice coverage) for the same period. Blue curves are the actual measures from the NRTSI data; orange ones show the IM simulation results.

5.2 Daily sea ice evolution in 2022

Do our semi-monthly IM simulation results match the actual sea ice dynamics on a smaller time scale? To answer this question, we utilize the semi-monthly Ising parameters in Table 1 to simulate the daily evolution in 2022. Two periods, a melting period from Aug 16th to Sept 1st, 2022, and a freezing period from Oct 16th to Nov 1st, 2022, are simulated day-by-day for this experiment. The results, with comparisons between the actual and the simulated daily ice evolution, are shown in Figure 8 to Figure 11. The comparisons exhibit striking similarity across all the daily images in both periods, confirming that our IM preserves the more granular ice/water dynamics.

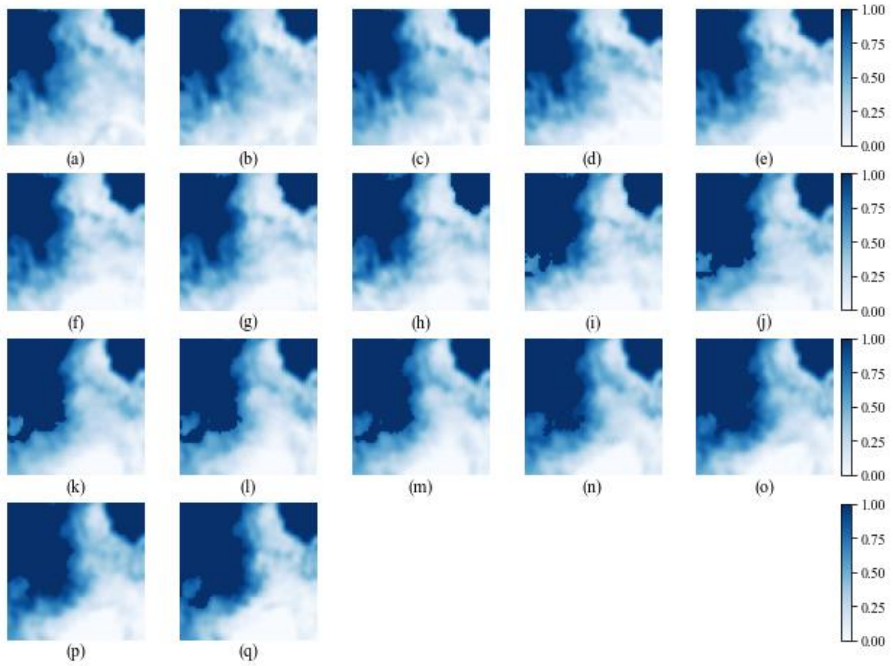

Figure 8: The actual daily evolution of sea ice in our focus area during a melting cycle from (a) Aug 16th to (q) Sept 1st, 2022.

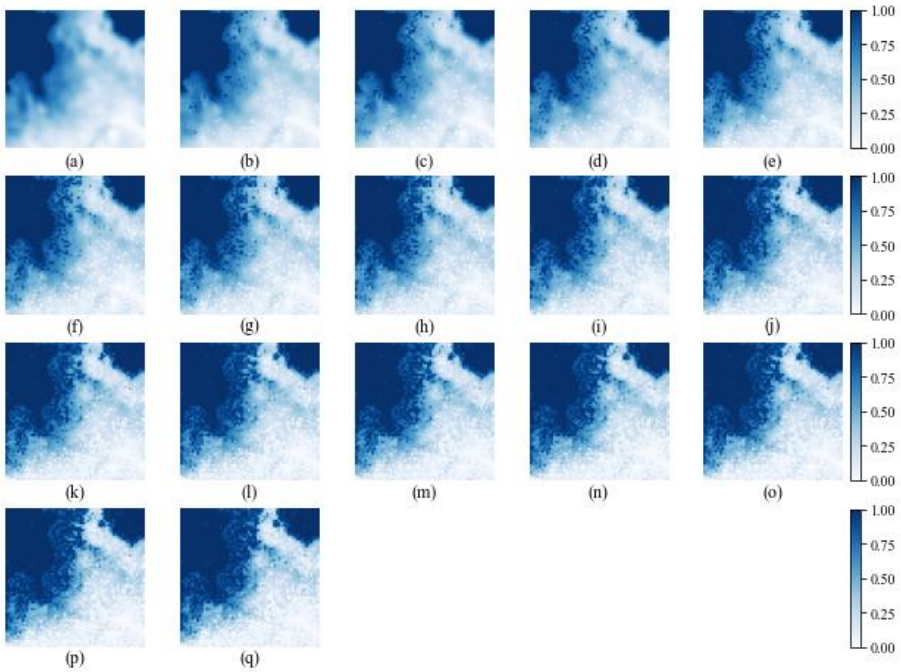

Figure 9: The simulated daily evolution of sea ice, based on the semi-monthly Ising parameters, for our focus area during a melting cycle from (a) Aug 16th to (q) Sept 1st, 2022.

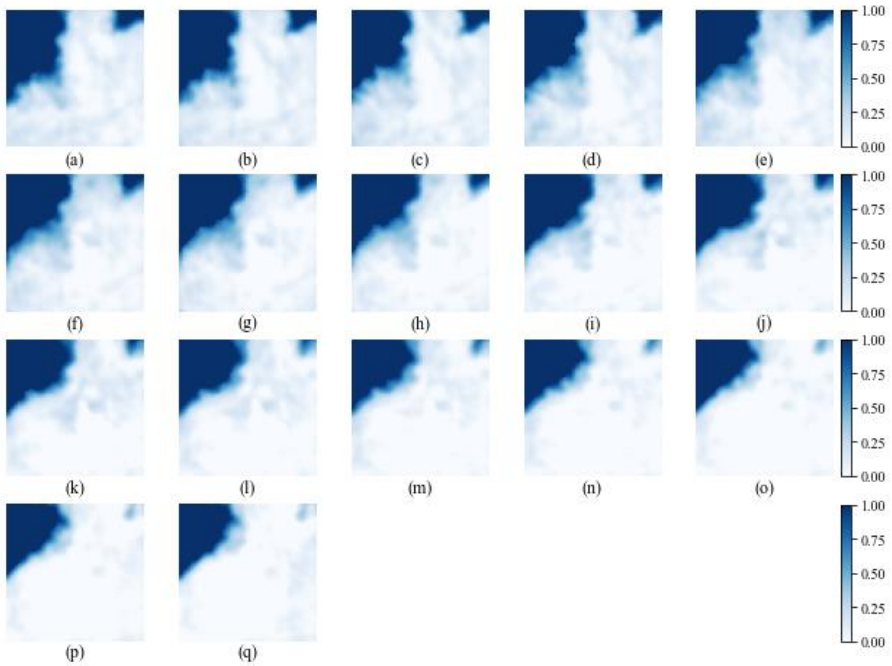

Figure 10: The actual daily evolution of sea ice in our focus area during a freezing cycle from (a) Oct 16th to (q) Nov 1st, 2022.

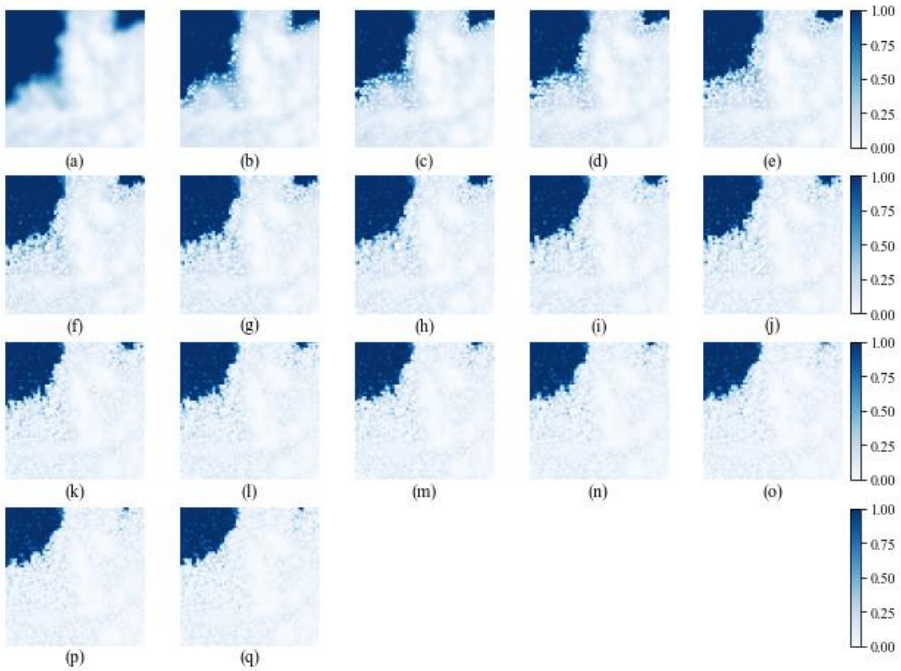

Figure 11: The simulated daily evolution of sea ice, based on the semi-month Ising parameters, for our focus area during a freezing cycle from (a) Oct 16th to (q) Nov 1st, 2022.

5.3 Simulation results for 2023

2023 has recorded the hottest year on record and is therefore a critical year for our study. Figure 12 shows the observed semi-monthly sea ice evolution from June 16th to Dec 1st in 2023 for our focus area. New data can certainly be included in this study in the future once it is collected. It can be observed that water covered approximately 75% of the area in peak September this year.

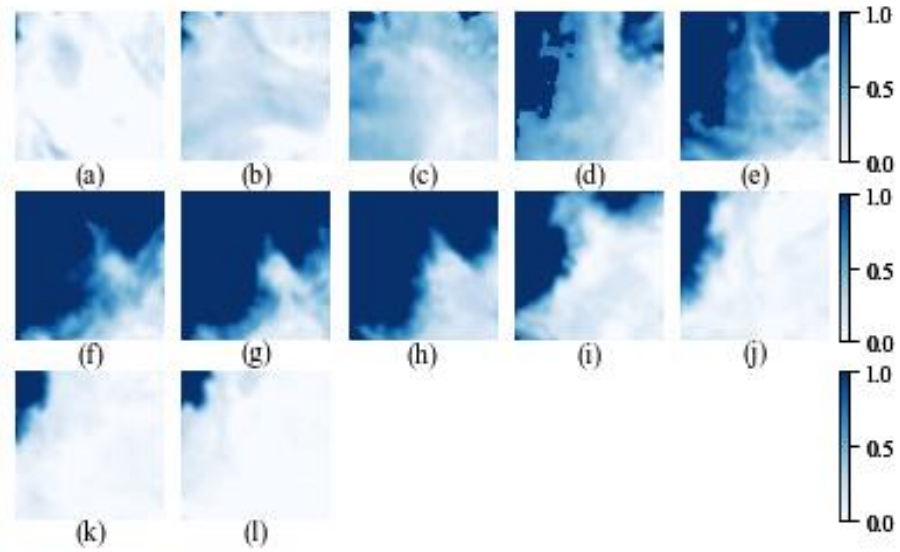

Figure 12: The actual semi-monthly evolution of sea ice in our focus area in 2023: (a) June 16th, (b) July 1st, (c) July 16th, (d) Aug 1st, (e) Aug 16th, (f) Sept 1st, (g) Sept 16th, (h) Oct 1st, (i) Oct 16th, (j) Nov 1st, (k) Nov 16th, and (l) Dec 1st

Following the same steps as in Section 5.1, the IM simulations and CNN training are conducted for 2023 for the focus area. The CNN predicted Ising parameters are listed in Table 2, the simulated images shown in Figure 13, and the comparisons for the average ice coverage percentage and the ice extent illustrated in Figure 14. Like the 2022 results in Section 5.1, excellent match is observed between the IM simulation and the actual sea ice evolution. As can be seen, the simulated sea ice extent drops to nearly 30% in Sept 2023 for our focus area, much lower than the September 2022 level in Figure 7.

	6/16 to 7/1	**7/1 to 7/16**	**7/16 to 8/1**	**8/1 to 8/16**	**8/16 to 9/1**	**9/1 to 9/16**	**9/16 to 10/1**	**10/1 to 10/16**	**10/16 to 11/1**	**11/1 to 11/16**	**11/16 to 12/1**
J	2.9	2.1	2.3	2.6	2.6	2.4	2.6	2.7	2.2	2.4	2.5
Bo	9.2	4.7	6.1	5.6	4.5	0.8	-3.9	-14.6	-15.5	-14.2	-15.9
Bx	-0.9	-0.8	-5.1	-4.6	-14.3	-2.0	2.2	-6.2	-9.0	-16.7	-9.2
By	-5.3	-1.0	-6.3	3.3	-15.3	4.8	-2.2	-5.5	-11.4	1.1	-6.1
I	12.7	7.9	10.3	10.9	10.6	9.3	10.7	9.8	8.5	9.7	9.8

Table 2: CNN predicted Ising parameters for the 2023 sea ice evolution.

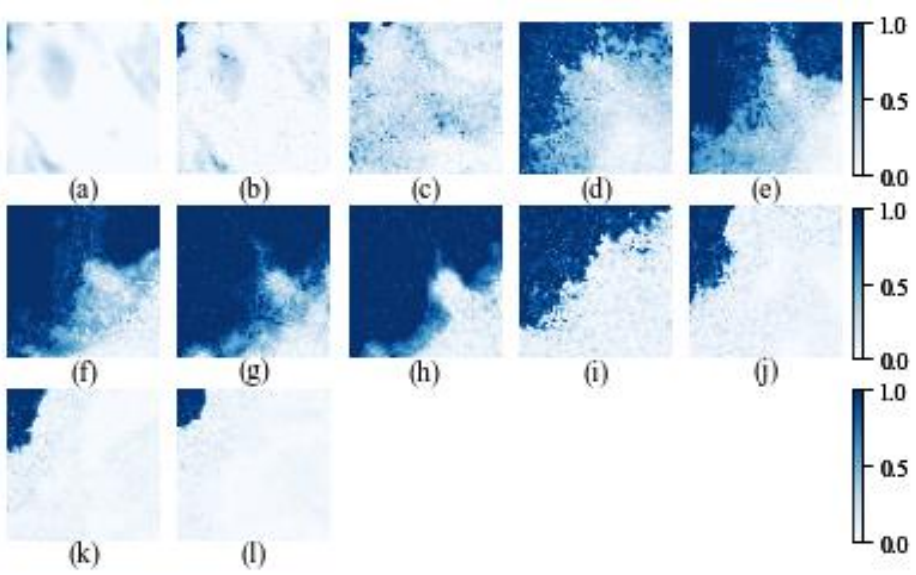

Figure 13: The simulated semi-monthly evolution of sea ice in our focus area in 2023. (a) is the actual image on June 16th; (b) - (l) are simulated images on (b) July 1st, (c) July 16th, (d) Aug 1st, (e) Aug 16th, (f) Sept 1st, (g) Sept 16th, (h) Oct 1st, (i) Oct 16th, (j) Nov 1st, (k) Nov 16th, and (l) Dec 1st.

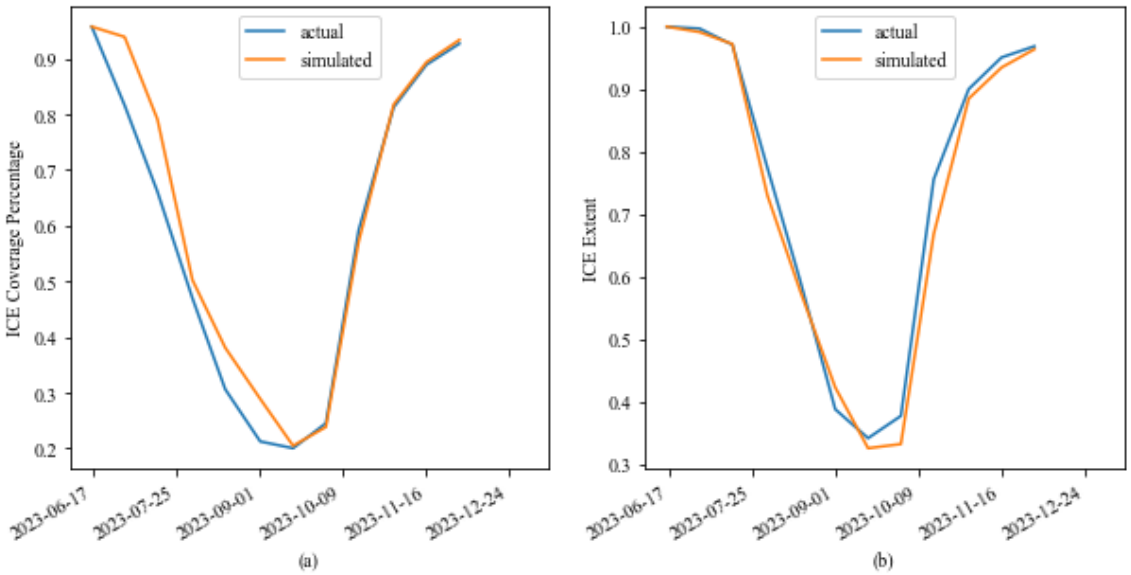

Figure 14: (a) The average ice coverage percentage in our focus area from June 16th to Dec 1st, 2023; (b) The sea ice extent (the percentage of areas with at least 15% ice coverage) for the same period. Blue curves are the actual measures from the NRTSI data; orange ones show the IM simulation results.

5.4 Comparison of sea ice extent between 2023 and 2012

2012 recorded the lowest September Arctic sea ice extent in history, while 2023 witnessed the hottest July and is projected to be the hottest year. It would be an interesting experiment to compare the 2023 sea ice extent to that in 2012.

Following the same steps as in Section 5.1 and Section 5.3, the IM simulations and CNN training are conducted for the period of June 16th, 2012 to Jan 1st, 2013 for the focus area. To keep our paper concise, we will skip the semi-monthly actual and simulated images and the CNN predicted parameters report. The more informative ice coverage and extent comparison charts are nevertheless included in Figure 15.

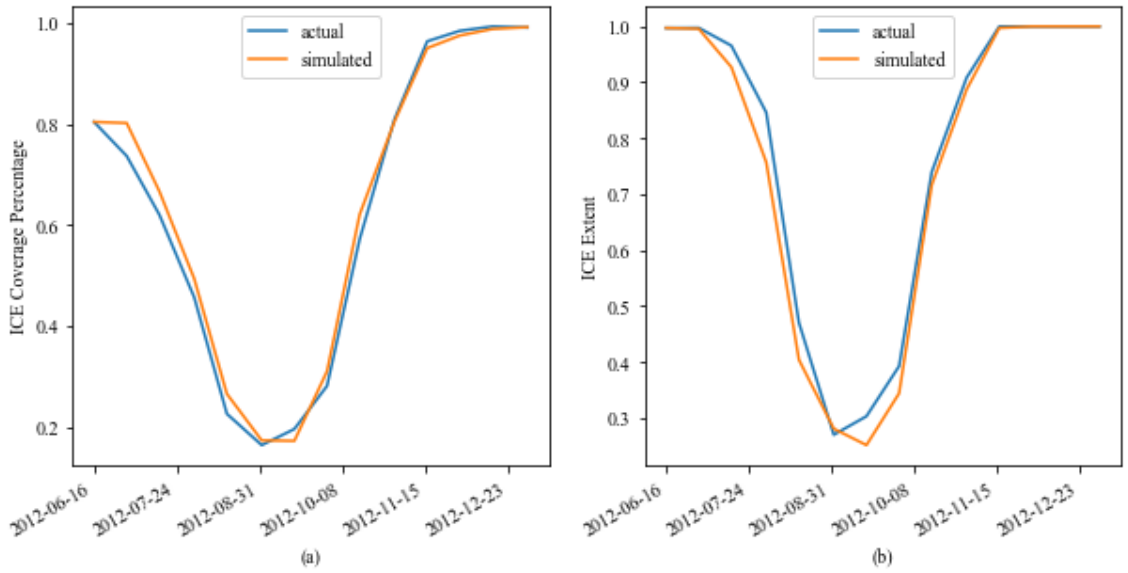

Figure 15: (a) The average ice coverage percentage in our focus area from June 16th, 2012 to Jan 1st, 2013; (b) The sea ice extent (the percentage of areas with at least 15% ice coverage) for the same period. Blue curves are the actual measures from the NRTSI data; orange ones show the IM simulation results.

Comparing Figure 14 with Figure 15 indicates that 2023 did not break the record-low Arctic sea ice extent level set in 2012, validated by both the actual measures and the IM simulations. However, 2023 sets the second lowest ice extent for our focus area, below those low levels previously achieved in 2019 and 2020[1] (2019 and 2020 results are not included in this paper but can be provided upon request.) Even though 2023 does not break the historical record, it offers no reason for us to be optimistic about the future. In fact, in the 45-year-satellite record from 1979 to 2023, 17 of the lowest minimums have all occurred in the last 17 years [22]. Many scientists are concerned that the effect of Arctic sea ice decline on global warming will intensify as the sea ice loss continues. Although

[1] For the entire Arctic region not limited to our focus area, 2023 marks the 6th-lowest ice extent in history [22]; all 6 minimums are well within small margins.

predicting the sea ice extent for the future years is beyond the scope of our current study, we will discuss the possibilities and issues in the next section.

6 Discussion and future work

In this paper, we innovatively introduce continuous spin values and an inertia factor to a classical 2-D IM, which is utilized to simulate the dynamics of the sea ice evolution in the Arctic region by employing the Metropolis-Hastings algorithm. A deep learning model based on CNNs is trained to solve the inverse Ising problem and obtain best-fit Ising parameters. Our results show excellent similarity with the actual sea ice dynamics, based on the ice configuration images and the numerical measures including the average ice coverage and the ice extent. It is exciting and inspiring to see that combining the 100-year-old classical Ising model with the modern innovations in deep machine learning has the potential to bring enormous power towards climate change research and other applied science studies.

6.1 Will a "Blue Ocean Event" happen? If so, when will it be?

Arctic sea ice extent in September 2023 was near the historic minimum achieved in 2012. As the Arctic sea ice continues to shrink, will a "Blue Ocean Event" happen, i.e., will we see an "ice-free" Arctic Ocean? Some research predicts that this can happen in the 2030s.

Our current study will need to be extended to gain the full predictive power when utilized to answer this "Blue Ocean Event" question. As shown in Table 1 and Table 2, the CNN predicted IM parameters demonstrate the substantial impact of the external force factor B, which remains unexplored within the scope of our model. If the functional form of this external force is further enriched and linked to actual environmental factors in climate change modeling, the IM framework may prove its strength in offering the "Ising Model Prediction" to answer the "Blue Ocean Event" question.

6.2 Larger machine learning model

The CNN model engaged in this study is fairly small (about 200,000 parameters only), and it is trained on the CPU of a personal computer. Yet, it has demonstrated amazing power to solve for the Ising parameters that explain the complex sea ice dynamics. A few straightforward technical enhancements can be considered in future research efforts, including but not limited to deeper and larger neural networks, and enriched Ising parameters, especially for the functional form of the external force factor B, to capture more details of sea ice dynamics.

6.3 Quantum Ising Model

Our study sets the stage for future Ising model research on sea ice evolution. Methodologically, we generalize the classical Ising model with continuous spin values to incorporate varying ice/water percentages across the Ising lattice. A more complicated idea to be explored in future research is the Quantum Ising Model (QIM), or the so-called Transverse Field Ising Model [23]. With quantum computers, the continuous spin values can be naturally modeled by the rotation of qubits in the Bloch Sphere. Large quantum computers are inaccessible for personal usage currently; but once they are reachable, our research can be readily extended with the assistance of quantum computing in the future.

7 Supplemental materials

7.1 IM and CNN results for other years

Detailed IM simulation and CNN results for 2012 will be provided upon request.

We also run analyses for the Arctic sea ice evolution in our focus area for other years; these results can also be provided.

7.2 Computer code and data

The computer programming for our research is done in Python. Source code and data can be shared upon request.

8 Acknowledgements

We thank the National Snow and Ice Data Center (NSIDC) and the National Aeronautics and Space Administration (NASA) for generously making the data publicly available and providing data support for this research.

We also thank Professor Joan Wang at the Xiamen University Malaysia Department of Physics for her inspiration, encouragement, and support, as well as Dr. Sergii Strelchuk at the University of Cambridge Department of Applied Mathematics and Theoretical Physics for his valuable guidance on machine learning studies and his crucial comments on this research.

In addition, we are grateful for the Science Research course by Dr. Alyssa Shearer at Horace Mann School for the introduction of various research methodologies and the access to extensive physics literature. We are also grateful for the Summer Research Program at the Western Connecticut State University Department of Mathematics for the learning opportunities of advanced simulation, optimization, and machine learning methods.

Bibliography

[1] E. Ising, "Beitrag zur Theorie des Ferromagnetismus," *Z. Phys,* vol. 31, no. 1, p. 2530258, 1925.

[2] L. Onsager, "Crystal statistics. I. A two-dimensional model with an order-disorder transition," *Physical Review,* vol. 65, no. 3-4, pp. 117-149, 1944.

[3] M. Aguilera, S. A. Moosavi and H. Shimazaki, "A unifying framework for mean-field theories," *Nature Communications,* vol. 12, p. 1197, 2021.

[4] B. Dun and Y. Roudi, "Learning and inference in a nonequilibrium Ising model with hidden nodes," *Physical Review E,* vol. 87, no. 2, p. 022127, 2013.

[5] J. Majewski, H. Li and J. Ott, "The Ising model in physics and statistical genetics," *The American Journal of Human Genetics,* vol. 69, no. 4, pp. 853-862, 2001.

[6] J. hertz, Y. Roudi and J. Tyrcha, "Ising model for inferring network structure from spike data," *In principles of Neural Coding,* pp. 527-546, 2013.

[7] Y. Roudi, D. B. and J. Hertz, "Multi-neuronal activity and functional connectivity in cell assemblies," *Curr. Opin. Neurobiol,* vol. 32, p. 38, 2015.

[8] Y. Shi and T. Duke, "Cooperative model of bacteril sensing," *Physical Review E,* vol. 58, no. 5, pp. 6399-6406, 1998.

[9] T. F. Stepinskia and J. Nowosad, "The kinetic Ising model encapsulates essential dynamics of land pattern change," *bioRxiv,* 2023.

[10] Y.-P. Ma, I. Sudakov, C. Strong and K. Golden, "Ising model for melt ponds on Arctic sea ice," *New Journal of Physics,* vol. 21, p. 063029, 2019.

[11] J. P. Bouchaud, "Crises and collective socio-economic phenomena: simple," *J. Stat. Phys.*, vol. 151, p. 567, 2013.

[12] S. Bornholdt and F. Wagner, "Stability of money: phase transitions," *Physica A: Statistical Mechanics and its Applications,* vol. 316, no. 1-4, pp. 453-468, 2002.

[13] J. Schmidhuber, "Annotated History of Modern AI and Deep Learning," *arXiv,* vol. 2212, p. 11279, 2022.

[14] Y. LeCun, B. Boser, J. S. Denker, D. Henderson, R. E. Howard, W. Hubbard and L. D. Jackel, "Backpropagation Applied to Handwritten Zip Code Recognition," *Neural Computation,* vol. 1, no. 4, pp. 541-551, 1989.

[15] G. S. Sylvester and H. van Beijeren, "Phase Transitions for Continous-Spin Ising Ferromagnets," *Journal of Functional Analysis,* vol. 28, pp. 145-167, 1978.

[16] M. Krasnytska, B. Berche, Y. YuHolovatch and R. Kenna, "Ising model with variable spin/agent strengths," *Journal of Physics: Complexity,* vol. 1, p. 035008, 2020.

[17] P. Basua, J. Bhattacharya, D. P. S. Jakkab, C. Mosomane and V. Shukla, "Machine learning of Ising criticality with spin-shuffling," *arXiv,* 2023.

[18] N. Walker, K. Tam and M. Jarrell, "Deep learning on the 2-dimensional Ising model to extract the crossover region with a variational autoencoder," *Scientific Reports,* vol. 10, p. 13047, 2020.

[19] G. S. Hartnett and M. Mohseni, "Self-Supervised Learning of Generative Spin-Glasses with Normalizing Flows," *arXiv,* 2020.

[20] J. Albert and R. H. Swendsen, "The Inverse Ising Problem," *Physics Procedia,* vol. 57, pp. 99-103, 2014.

[21] W. N. Meier, J. S. Stewart, H. Wilcox, M. A. Hardman and S. D. J., "Near-Real-Time DMSP SSMIS Daily Polar Gridded Sea Ice Concentrations, Version 2," NASA National Snow and Ice Data Center Distributed Active Archive Center, Boulder, Colorado USA, 2023.

[22] "Arctic sea ice minimum at sixth lowest extent on record," National Snow & Ice Data Center,, 2023. [Online]. Available: https://nsidc.org/arcticseaicenews/2023/09/arctic-sea-ice-minimum-at-sixth/.

[23] B. K. Chakrabarti, A. Dutta and P. Sen, Quantum Ising Phases and Transitions in Transverse Ising Models, Berlin: Springer, 1996.